https://doi.org/10.5194/hess-2022-275
Preprint. Discussion started: 10 August 2022

Hydrology and Earth System Sciences
Discussions
Open Access

Resistance parameters and permissible velocity from cohesive channels

Jose Ramon B. Cantalice[1], Layane Carmem A. Rocha[1], Carlos V.O. Alves[1], Amanda Q. L. Moura[1], Edgo J. P. Santiago[2], Maykon R. G. Barros[1], Paulo Costa Medeiros[3]

[1] Soil Conservation Engineering Laboratory, Environmental Engineering Program, Rural Federal University of Pernambuco (UFRPE), Recife-PE, Brazil;
[2] Biometry and Applied Statistics Program, Rural Federal University of Pernambuco (UFRPE), Recife-PE, Brazil
[3] Federal University of Campina Grande, Sume Campus, Sume-PB, Brazil.
Corresponding author: Jose Ramon B. Cantalice, e-mail: ramoncanta21@gmail.com

ABSTRACT

The forces determining erosion resistance in cohesive channels are not yet completely understood. Therefore, this study aimed to evaluate the resistance parameters and obtain a flow velocity equation for such channels. Experimental data were obtained from cohesive channels with a 60% clay proportion and under increasing flow levels. The soil detachment rates were inversely proportional to the applied shear stress, and the obtained critical shear stress and soil erodibility values were as high as 120 Pa and 0.00003 kg N^{-1} s^{-1}, respectively. Under the highest applied flow, the yield stress was significantly influenced by the geometry variation, flow velocity, and sediment concentration. The shear stress generated by the applied flows remained below the critical shear stress of the cohesive bed channels. Using the Buckingham theorem, we developed an equation to predict the permissible flow velocity in cohesive channels. this will help engineers design and manage river structures more effectively.

Keywords: dimensional analysis, shear stress, cohesive erodibility, resistance to direct shear stress, critical shear stress, yield stress, cohesive beds.

1. Introduction

The permissible velocities applied in conventional methods predict the constant shear stress and flow velocity using practical engineering principles that can vary between projects (Qasem et al., 2017). Furthermore, Utley and Wynn (2008) predicted erosion

https://doi.org/10.5194/hess-2022-275
Preprint. Discussion started: 10 August 2022

rates under cohesive conditions by using the interactions between the water contained in the porous soil and the eroding flow, as well as the cohesive properties of the soil.

Detachment processes can occur in cohesive sediment within channels, earthen dams, and spillways; these are modeled using an linear approach to determine the shear stress. Hence, engineers require methods to quantify water erosion under cohesive conditions (Khanal et al., 2016). Partheniades (1965) first modeled cohesive erosion rates using the excess shear stress:

$$\varepsilon_{r=K_d}(\tau-\tau_c)^a. \tag{1}$$

Here, ε_r is the erosion rate, K_d is the erodibility coefficient, τ is the flow shear stress, τ_c is the critical shear stress, and *a* is the exponent, which is taken as unity. In this model, the erosion rates are proportional to the difference between the applied shear stress and boundary critical shear stress.

The erosion rates of overland flow on rangelands tend to be relatively low; however, where the flow is concentrated, soil loss can be significant. Therefore, a cropland site can be susceptible to concentrated flows when excess shear stress is placed on the soil particles. This concept has been applied to crops in agricultural areas and hydrological soil erosion events around the world (Al-Hamdan et al., 2013).

Concentrated flows consist of storm water flowing within a confined geomorphic landscape feature such as a rill, channel, or river. De Baets et al. (2006) reported that in the 1990s, important advances were made toward understanding concentrated flow erosion and its hydraulic behavior under environmental conditions that may result in the formation of rills and gullies.

Aliev (1985) stated that when erosion processes occur in cohesive channels, detachment occurs for all stretches of the drain system and continues throughout the channel. In this situation, the transport capacity is incomplete, in contrast to the deformation processes in the sand channels.

Because cohesive sediments feature a large specific area (owing to the small sizes of clay particles), physicochemical forces act as cation and hydrogen bonds to ensure cohesion between clay particles; however, these factors have not been widely studied in situations where the soil undergoes applied shear stress and increased soil moisture (Ansari et al., 2003).

For cohesionless sediments, the primary resistance to erosion is provided by the submerged weight of the sediment. In cohesive beds, the net attractive interparticle surface forces, frictional interlocking of grain aggregates, and electrochemical forces all control the resistance to erosion and detachment. These forces vary with the type of clay, antecedent moisture conditions, type of shear applied, and drainage conditions (Ansari et al., 2003). Therefore, these forces are not completely understood. The main mechanisms that cause sediment to move in flowing water are the flow velocity, shear, and normal stress resulting from flow turbulence (Jain and Kothyari, 2009).

Sekine et al. (2008) reported that only minimal information is available regarding the erosion rates of cohesive sediments via water surfaces, and the erosion mechanisms of cohesive sediments are not entirely understood. However, researchers have asserted that clay particles combine owing to the complicated mechanism of cohesive force applied to their surfaces. Engineers must know the quantity of deposited cohesive sediment that can be detached or transported under specific shear stresses, to facilitate effective management of river structures (e.g., dams and sluice gates) and water transport facilities and the proper design of stable channels in cohesive sediment.

Mirtskhoulava (1991) stated that water erosion is an extremely relevant aspect of hydraulic design: appropriate designs can restrict flow velocities to below the permissible level, to prevent water erosion; such designs represent a target of fluvial hydraulics. However, because of their mineralogical and chemical characteristics (and subsequent mechanical and physical behaviors), predicting the resistance of cohesive soils is more complicated than that of sandy soils, for the resistance under these conditions depends solely on the particle weight. This complexifies the designing of hydraulic structures in cohesive soils.

To understand the incipient motion of cohesive sediments, several factors pertaining to the flow acting on the boundary and the cohesive material’s boundary must be understood. Zhang and Yu (2017) reported that cohesive sediment transport depends on the rheological properties of the sediment, and they introduced the yield stress (τ_y) concept. This stress is produced when a shear stress acts on a soil or sediment sampler, thereby changing its state from solid to liquid and causing it to flow. The stress is proportional to the interparticle interactions. Yield stress can also occur when a sample is subjected to normal stress in a direct shear test that produces shear stress. Zhang et al.

https://doi.org/10.5194/hess-2022-275
Preprint. Discussion started: 10 August 2022

(2017) claimed that the primary factor determining cohesive sediment erodibility is yield stress.

Zhang and Yu (2017) presented an empirical expression for the onset of movement for a cohesive sediment (Θ_{cr}), which they developed via dimensional analyses to produce a dimensionless yield stress parameter (τ_r), expressed as

$$\tau_r = \frac{\tau_y}{\rho_s (\nu g)^{\frac{2}{3}}} \,, \tag{2}$$

where ρ_s is the particle density (kg m^{-3}), g is the gravitational acceleration (m s^{-2}), υ is the kinematic viscosity of flow (m^2 s^{-1}), and τ_y is the yield stress (N m^{-2}). Zhang and Yu (2017) assumed that (Θ_{cr}) corresponded to an exponential function of the yield stress (τ_y) and dimensionless particle diameter (D_*); thus, the increase of (Θ_{crc}) became progressively weaker; as a result, the rheological term reflected the yield stress influence on Θ_{crc}, calculated as

$$\theta_{cr_c} = (0.056 - 0.033e^{-0,0115D_*} + 0.12e^{-0,25D_*} + 0.48e^{-3,8D_*}) \times \left(e^{9.8\times10^{-4}\times\tau_r\times\exp(-0.4D_*)}\right). \tag{3}$$

The erodibility (K) and critical shear stress (τ_c) were also used as resistance parameters for the cohesive sediments. Mahalder et al. (2018) tested different pressure levels on soils with clay contents of 15–25%, to obtain the maximum critical shear stress (τ_c), which varied from 12.43 to 26.80 Pa; maximum erodibility values (K) of 3.84–24.2 cm^3 $N^{-1}S^{-1}$ were also obtained.

Graf (1984) noted that the relation for shear stress in a cohesive material can be written as

$$\frac{\tau_0}{(y_s - y)d} = A_1'' + C_0, \tag{4}$$

where τ_0 is the shear stress; y_s and y are the sediment- and soil-specific weights, respectively; d is the average diameter of the grain; A_1'' is the sediment coefficient; and C_0 is the coefficient of cohesion for the material. The coefficient A_1'' can be omitted for materials where the cohesive forces are much larger than the other forces. However, in soil mechanics, the shear stress corresponding to a failure can be approximated by

$$\tau = \sigma \tan\phi + C, \tag{5}$$

https://doi.org/10.5194/hess-2022-275
Preprint. Discussion started: 10 August 2022

where τ is the shearing strength or shearing resistance, σ is the effective pressure, and C denotes the cohesion. This equation is known as *Coulomb's* equation and is similar to Eq. 4. The cohesion at saturation water content, dispersed particle size, and soil aggregate stability (i.e., the soil's resistance to water) appear to be the most important elements of the extensive and complex physical and mechanical properties of cohesive soils. Consequently, Mirtskhoulava (1996a) reported that resistance to scouring increases under an increase in cohesive strength, owing to the moisture content.

This study aimed to evaluate the parameters of erosion resistance, including the cohesion, soil erodibility, critical shear stress, and yield shear stress of highly cohesive channels. In addition, to obtain a flow velocity equation for cohesive channels, we applied dimensional analysis to experimental data, considering the hydraulic and cohesive parameters governing the concentrated flow velocity under these conditions.

2. Material and Methods

This study was performed in the Experimental Station of Rural Federal Pernambuco University located in Carpina city, Pernambuco state, Brazil (7º 51' 13" S, 35º 14' 10" W) (Figure 1), 180 m above sea level. The climate in the study area has a Köppen climate classification as "Ams,"; which is a rainy tropical climate with dry summers (less than 60 mm in the driest month) and the total precipitation is 1200 mm.year^{-1}. This area has been cultivated with Sugarcane crops for more than 400 years, and the native vegetation was the Atlantic Forest. The experiment was located on the landscape medium part with a slope between 0.13-0.16 m.m^{-1}, under a Ultisol according to the Soil Taxonomy USDA (1998), with a sand surface horizon of 40 cm depth and an Argillic B horizon with a 60% clay proportion. The soil attributes are enclosed in tables 1 and 2.

https://doi.org/10.5194/hess-2022-275
Preprint. Discussion started: 10 August 2022

Hydrology and Earth System Sciences
Discussions
Open Access

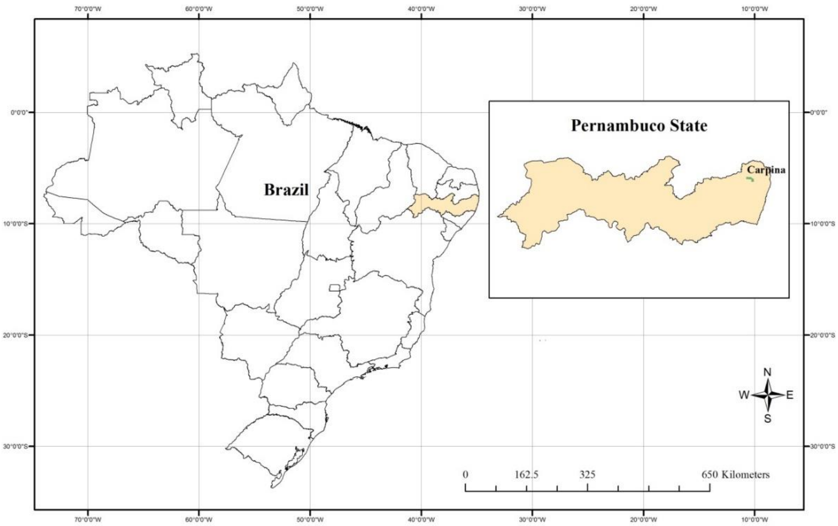

Figure 1. Sugarcane Experimental Station of the Rural Federal University of Pernambuco, located in Carpina City, Pernambuco State, Brazil. Map entirely created by authors.

Table 1. Some physical attributes of the horizon B of a Ultisol from Brazil. Soil density (ρ), particle density (ρ_s), total porosity (α), and water content. Average values considering four repetitions.

ρ_d	ρ_p	α	θ
----- kg m^{-3} -----		----- m^3 m^{-3} -----	
1381	2675	0.484	0.356

Table 2. Particle size distribution, organic carbon content, and soil texture of the horizon B of a Ultisol from Brazil. Average values considering four repetitions.

Treat.	OC	Sand	Silt	Clay	Textural classification
	%	------- g kg^{-1} -------			
1	0.54	187.75	247.56	564.70	Clay
2	0.45	122.72	211.78	665.50	Clay
3	0.51	167.33	201.59	631.08	Clay

https://doi.org/10.5194/hess-2022-275
Preprint. Discussion started: 10 August 2022

4	0.69	173.55	217.31	609.15	Clay

Organic carbon analysis was performed using the dry combustion method, and the soil density (ρ) was determined using the methodology of Grossman and Reinsch (2002). The particle density (ρ_s) was obtained according to Blake and Hartge (1986), and the total porosity (α) was calculated following Flint and Flint (2002). Table 1 summarizes the results of the physical analyses.

2.1 Pre-formed cohesive channels and experimental procedure

The bed channels had a soil texture with a high clay content (Table 2), which was pre-formed under the B-horizon of the Ultisol. Initially, the Ultisol surface soil horizon was removed and deposited adjacent to the experimental area (Figure 2). Then, 16 channels were pre-formed; these consisted of four larger channels of width 0.5 m, depth 0.2 m, and length 4 m and 12 smaller channels of width 0.1 m, depth 0.05 m, and length 4 m. A gutter was placed at the lower end of the channels to sample water and solid discharges. Water was added to the channels by pipes connected to a water reservoir maintained at a constant level. These cohesive channels were applied at the following flow levels: Q_1 = 70, Q_2 = 132, and Q_3 = 210 for smaller channels, and Q_4 = 545 L min^{-1} for larger channels. All tests lasted for 20 min.

Figure 2. Cohesive channel preparation under a cohesive horizon of a Ultisol. Figure from authors.

The mean flow velocities for all cohesive channels were obtained using an electromagnetic current meter and the dye method. For the dye method, methylene blue was introduced at the start of the channels, and the time taken for the dye to reach the channel's outlet was measured using a chronometer. The channel length divided by the time taken by the dye yielded the superficial velocity (*Vs*) of the flow and was expressed in m s^{-1}. In this procedure, the superficial velocity values were multiplied by $\alpha = 2/3$; then, a correction factor was applied, and the mean velocity (V_m) was ultimately recorded in m s^{-1} (Farenhorst and Bryan, 1995; Cassol et al., 2004; Cantalice et al., 2017).

The water discharge (*Q*) was computed from the sampling runoff obtained in plastic pots placed on the channel outlets at 5-min intervals; this was obtained concomitantly with flow velocity measurements. A linear ruler was used to measure the flow depth (h) (cm) for larger channels, and a profilometer was used to take the hydraulic radius (R_h) (m) for the smaller channels, as well as the channel area (*A*) (m^2). The kinematic viscosity was determined using the equation proposed by Julien (1995), in which we used the water temperature (°C) measured by a thermometer in each test. The Froude number (Fr) and Reynolds number (Re) were obtained according to Simons and Senturk (1992).

The Darcy–Weisbach coefficient (*f*) was used to express the hydraulic resistance:

$$f = \frac{8gR_hS}{V^2}. \quad (6)$$

Here, *f* is the Darcy–Weisbach coefficient (dimensionless), R_h is the hydraulic radius (m), *S* is the water surface slope (m m^{-1}), *V* is the mean flow velocity, and g is the gravitational acceleration (m s^{-2}).

2.2 Mirtskhoulava's permissible velocity

Mirtskhoulava´s permissible (Mirtskhoulava, 1996a, Mirtskhoulava, 1991) velocity was used to verify the equation's performance on cohesive channels, mainly through a paired comparison to velocity values obtained by an electromagnetic current meter within the channels. Mirtskhoulava's equation (1991) is expressed as

$$V = log_{10}\frac{8.8R_h}{d}\sqrt{\frac{2gm}{2.6\gamma n'}\left[(\gamma_s - \gamma)d + 1.25C_fK\right]}, \quad (7)$$

where V is the permissible velocity (m s^{-1}), R_h is the hydraulic radius (m), d is the median surface grain diameter (D_{50}, mm), g is the acceleration due to gravity (m s^{-2}), and m is the working condition coefficient, which expresses the influences of different factors on the operating conditions and is usually considered equal to 1 for recently prepared soils. γ and γ_p are the specific weights of water and sediment (t m^{-3}), respectively; and n' is the overload coefficient considering the change in scouring flow capacity (which is influenced by pulsating velocities and other probable cases of loads exceeding their calculated values). The overload coefficient it is obtained from the following expression:

$$n' = 1 + \frac{d}{0.00005+0.3d}. \quad (8)$$

Here, C_f is the soil fatigue strength needed to rupture (Pa); it is a function of soil cohesion, obtained via

$$C_f = 0.035C, \quad (9)$$

where C is the soil cohesion (Pa) obtained by direct shear tests, and K is the clay soil homogeneity coefficient, which characterizes the probability that the cohesion indices deviating unfavorably from their mean values; this coefficient is obtained from

$$K = 1 - \frac{\alpha\sigma}{C}, \quad (10)$$

where α is a coefficient characterizing the minimum probability of soil resistance or the safety coefficient [usually taken as 3 (Mirtskhoulava, 1966a)], and σ is the standard deviation of the data.

2.3 Detachment rates for concentrated flow in cohesive channels

The soil detachment rates under the concentrated flow conditions were calculated to the level needed to overcome the critical shear stress arising from the cohesive channel, based on the methods of Partheniades (1965), Elliot et al. (1989), Flanagan and Nearing (1995), and Thoman and Niezgoda (2008), as follows:

$$D_c = K(\tau - \tau_{cr})^1. \quad (11)$$

Here, D_c is the detachment capacity (kg m^{-2} s^{-1}), K is the erodibility of the soil (kg N^{-1} s^{-1}) in response to shear stress τ (N m^{-2} or Pa), and τ_c is the critical shear stress of the soil (N m^{-2} or Pa). Therefore, the shear stress τ was obtained as

$$\tau = \gamma R_h S, \quad (12)$$

https://doi.org/10.5194/hess-2022-275
Preprint. Discussion started: 10 August 2022

Hydrology and Earth System Sciences Discussions
Open Access

where γ is the specific weight of water (N m^{-3}), R_h is the hydraulic radius (m), and S is the soil surface slope (m m^{-1}). According to Partheniades (1965), the cohesive bed erodibility (K) is considered as the angle coefficient b of a linear regression model between the soil detachment rate and shear stress τ, and the critical shear stress (τ_c) corresponds to the intercept value of τ, where the detachment rate D = 0.

The soil detachment rates from the concentrated flow were obtained from sediment sampled every 5 min using (Flanagan and Nearing, 1995)

$$D = \frac{QC}{LP_w}, \tag{13}$$

where D is the soil detachment rate in response to the concentrated flow (kg m^{-2} s^{-1}), Q is the flow rate (L s^{-1}), C is the sediment concentration (kg L^{-1}), L is the length of the channel (m), and P_w is the cohesive channel width (m).

2.4 Sampling for mechanical soil analysis

Disturbed soil samples were collected on the cohesive bed channels, air-dried, and sieved through a 2 mm mesh. Thirty-two undisturbed soil samples were collected and placed into a rectangular stainless-steel box (0.06 × 0.06 × 0.043 m) encased in bubble plastic, to ensure proper readings of the cohesive channels' physical and mechanical parameters.

The direct shear test was performed according to the norm D-3080/98 of the American Society for Testing and Materials (ASTM D 3080-98, 2003); this was conducted using a direct shear press device with a shear velocity of 0.125 mm min^{-1}. The normal pressures used during the tests were 50, 100, 150, and 200 kPa. At the end of the test, the data required for the equations:

$$\sigma_n = \frac{N}{a}, \tag{14}$$

(where σ is the normal stress, N is the normal force applied to the test body, and a is the transverse section area of the sample) and

$$\tau_c = \frac{T}{a}, \tag{15}$$

(where τ_c is the shear stress and T is the force applied to the test body) were obtained.

Soil cohesion (C) was determined using the value of direct shear stress under each normal stress at the end of the test, by plotting the relation between the two. The cohesion values were obtained from the intercept of the equation for the line formed in the graph.

2.5 Shields critical parameter for cohesive sediment (Θ_{cr})

In the Shields critical parameter for cohesive sediment (Θ_{cr}) determination, the dimensionless yield stress parameter (τ_r) was incorporated according to Zhang and Yu (2017) and defined by Eq. (2). The yield stress values (τ_y) were obtained from direct shear stress tests on bed cohesive samples under saturated conditions, which consisted of the shear stress observed when the bed cohesive samples were subjected to different normal stress levels. The numerical calculation of the Shields critical parameter for cohesive sediment values (Θ_{cr}) was obtained using Eq. (3), where the dimensionless particle diameter (D_*) was obtained using

$$D_* = d_{50}\left[g\left(\frac{\rho_s-\rho}{\rho\upsilon^2}\right)\right]^{\frac{1}{3}}, \quad (16)$$

where d_{50} is the size diameter (m), ρ_s is the particle density (kg m^{-3}), ρ is the water density, g is the gravitational acceleration (m s^{-2}), and υ is the kinematic viscosity of flow (m^2 s^{-1}).

2.6 Dimensional analysis

The dimensional analysis was based on the Buckingham π theorem and the repeated variable method (Fox et al., 2015). This analysis is based on the difference between the number of dimensional variables that describe a process (k) and the number of dimensions that reference these variables (r); this results in the group's dimensionless number (denoted as π). A set of fundamental dimensions is used as a reference, such as [mass] = M, [length] = L, and [time] = T (Dym et al., 2010). Initially, the dependent and independent variables were defined according to

$$q_1 = f(q_2, q_3, q_4, \ldots q_n). \quad (17)$$

The theorem establishes that it is possible to adjust the relationship between n variables, as follows:

$$q(q_1, q_2, q_3, q_4 \ldots q_n) = 0 \;. \quad (18)$$

These n variables can be grouped into k – n independent dimensionless ratios, or π parameters, which are expressed in a functional form as

https://doi.org/10.5194/hess-2022-275
Preprint. Discussion started: 10 August 2022

$$G(\pi_1, \pi_2, \pi_3, \pi_4, \ldots \pi_{k-n}) = 0, \quad (19)$$

and rewritten according to

$$\pi_1 = G_1(\pi_2, \pi_3, \pi_4, \ldots \pi_{k-n}). \quad (20)$$

After determining the number of π groups observable, a dimensional parameter set describing all primary dimensions was established based on the procedures of Fox et al. (2014); these parameters are referred to as repeating parameters (m); typically, m = r. Thus, the repeated parameters were combined with the remaining ones.

Based on Díaz (2012), we investigated whether an observed variable belonged to the π group. The first task was to place dimensionless variables in a π group, and the second was to designate any two variables of identical dimensions as constituting a π group. Finally, the dimensional groups were resolved and made dimensionless (Munson et al., 2004).

2.7 Statistical analysis

This study was conducted in a randomized block with four treatments (four flow levels) and four repetitions, totaling 16 cohesive experimental channels. The data were initially analyzed using descriptive statistics to identify outliers that could compromise the behavior of the studied parameters; then, the data were subjected to a two-way analysis of variance. Other tests were also applied, such as the Kolmogorov–Smirnov and Shapiro–Wilk tests, to verify data normality; the F test, for variance analysis; and the Tukey test, to obtain a mean comparison between treatments at a 5% probability.

3. Results and Discussion

3.1 Hydraulic behavior of the larger cohesive channels under the applied flow

Table 3 summarizes the hydraulic behavior obtained from the four larger cohesive channels, in which the mean flow velocity was obtained for the applied flow levels. In all tests, the Reynolds numbers were turbulent, and the Froude number values showed a slow or tranquil flow. The obtained hydraulic radius was between 0.055 and 0.59 m, which meant that all channels could reach similar areas. Descriptive statistics confirmed the homogeneity of the generated flows.

Figure 3 shows the mean velocity behavior, as measured using the electromagnetic current meter and dye method under the applied flows within the larger cohesive channels; a high correlation coefficient was obtained for the paired velocities when compared to the velocities obtained under these two methods.

https://doi.org/10.5194/hess-2022-275
Preprint. Discussion started: 10 August 2022

Table 3. Hydraulic variables under applied flows on larger cohesive channels under a cohesive B horizon of the studied Ultisol in Brazil. Average values considering four repetitions, n = 16.

Variables	Applied flows			
	Run 1	Run 2	Run 3	Run 4
Q ($m^3 s^{-1}$)	0.00897	0.00713	0.00708	0.00593
τ (Pa)	93.89	88.37	76.20	55.74
V_m ($m s^{-1}$)	0.4987	0.5044	0.3497	0.5988
Re (Adm.)	33060.85	31471.87	23771.38	40403.02
Fr (Adm.)	0.659	0.687	0.456	0.784
f	2.97	2.73	4.90	1.22
P_m (m)	0.964	0.831	1.023	1.006
R_h (m)	0.0584	0.0550	0.0599	0.0595
A (m^2)	0.0555	0.0450	0.0604	0.0590
S ($m m^{-1}$)	0.1611	0.1611	0.1275	0.0940

All variables were normal distribution by the Kolmogorov test at 5% probability.

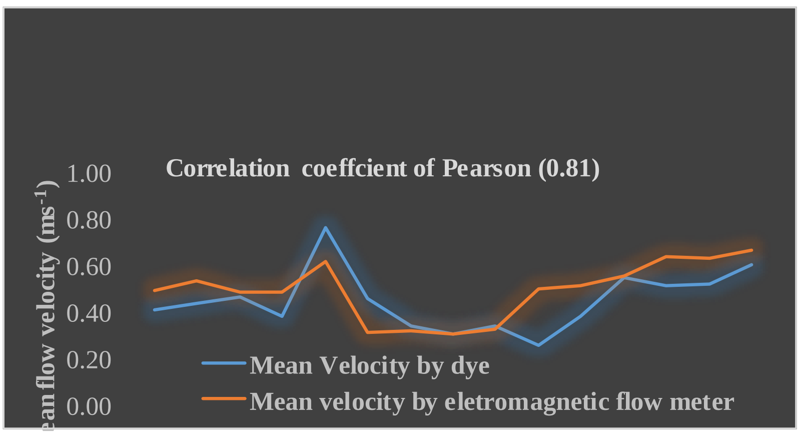

Figure 3. Relationship between mean velocities measured by the electronic current meter and by dye method on cohesive channels under different flows applied. Average values considering four repetitions and n (runs number) = 16.

In the cohesive channels under applied flows, the resistance hydraulic (represented by the Darcy–Weisbach coefficient) showed an inverse response to the mean flow velocity (Figure 4), , indicating that the shear stress response to the flow influenced

https://doi.org/10.5194/hess-2022-275
Preprint. Discussion started: 10 August 2022

Hydrology and Earth System Sciences
Open Access
Discussions

the mean velocity via the residual energy. The shear stress level obtained was comparable to that of a cohesive bed with a high clay content, as observed by Thoman and Niezgoda (2008) and Grabowski et al. (2010).

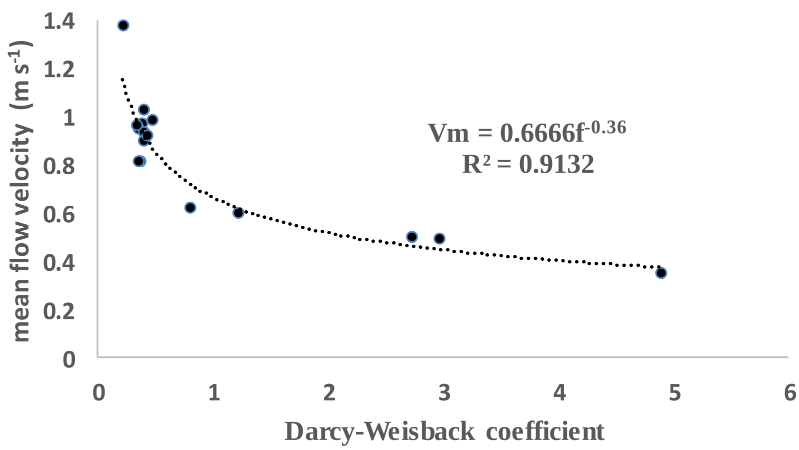

Figure 4. Relationships between mean flow velocity (V_m) and resistance hydraulic represented by Darcy-Weisbach (*f*) on cohesive channels under different flows applied. Average values considering four repetitions and n (runs number) = 16.

3.2 Hydraulic behavior of all cohesive channels for all levels of applied flow

Table 4 summarizes the hydraulic behavior observed in the smaller cohesive channels in response to the different applied flows. Because of the significant increase in the applied flow, the channel geometry was altered by increasing the wetted perimeter and area. This allowed for the differentiation of the hydraulic radii and, thereby, an ultimately significant increase in the obtained shear stress (τ).

https://doi.org/10.5194/hess-2022-275
Preprint. Discussion started: 10 August 2022

Table 4. Hydraulic variables channels of cohesive channels for different levels of applied flows on cohesive channels. Average values considering four repetitions.

Hydraulic Variables[1]	Different levels of applied flows.			
	Q_1	Q_2	Q_3	Q_4
Q (L min^{-1})	49.97a	66.01 ab	72.13 b	436.52 c
τ (Pa)	35.64 b	46.62 b	49.08 b	78.55 a
Re (Adm.)	23073.71 b	31335.26 ab	39040.01 a	32176.78 ab
Fr (Adm.)	1.58 a	1.84 a	1.88 a	0.64 b
f	0.482 a	0.388 a	0.363 a	2.956 b
V_m (m s^{-1})	0.7895 ab	0.9703 a	1.0617 a	0.4879 b
P_m (m)	0.1319 a	0.1682 ab	0.2282 b	0.9558 c
R_h (m)	0.0256 a	0.0284 ab	0.0322 b	0.0582 c
A (m^2)	0.0034 a	0.0047 ab	0.0073 b	0.055 c
S (m m^{-1})	0.1396 a	0.1644 a	0.1528 a	0.1359 a

[1]Means followed by the same small letter did not differ in column (Tukey, $p < 0.05$).

The flow regimes for all channels were turbulent and slow according to the Reynolds and Froude numbers, respectively. This is in accordance with the findings of Simons and Senturk (1992), who reported that this dynamic frequently occurs in natural alluvial channels. However, the Froude and Reynolds numbers showed a significant increase under the applied flow. Following Slattery and Bryan (1992) and Bezerra et al. (2010), we noted whether any of the cohesive channels achieved a Froude number of 2.8. The hydraulic resistance obtained for the Darcy–Weisbach coefficients was only significant for higher applied flows, most likely attributable to the high clay content of the cohesive channels.

3.3 Resistance and rheological parameters of cohesive channels: critical shear stress, yield stress, and channel erodibility

Table 5 summarizes the average values for the soil detachment rate (D), sediment concentration (C_s), dimensionless particle diameter (D*), yield stress (τ_y), dimensionless yield stress (τ_r), and Shields critical parameter, as obtained from cohesive agricultural channels. As observed in Table 4, significant differences occurred for higher applied flows when the yield stress and dimensionless yield stress parameter (τ_r) were different. However, these values were obtained from the saturated direct shear stress, thereby demonstrating the exact behavior of the cohesive channels under the flow-generated shear

https://doi.org/10.5194/hess-2022-275
Preprint. Discussion started: 10 August 2022

Hydrology and Earth System Sciences
Discussions

stress. Therefore, the yield shear showed an exact difference when the flow shear stress, channel geometry, and hydraulic resistance were altered at the highest flow level applied. Zang and Yu (2017) indicated that yield stress is primarily related to incipient movement under cohesive sediment conditions.

Table 5. Resistance parameters of the cohesive agricultural channels: Cohesion (C), failure cohesion (C_f), critical shear stress (τ_c), soil erodibility (K), yield shear stress (τ_y), dimensionless yield shear stress parameter (τ_r), and Shields's parameter to cohesive sediment (Θ_{cr}) for the applied concentrated flows. Average values considering four repetitions.

D_r (kg m^{-2} s^{-1})	C_S (kg m^{-3})	D_*	τ_y (Pa)	τ_r	θ_{cr}
0.003a	1.986a	0.005158a	147.33a	13.36a	0.639a
0.002a	1.741a	0.005415a	148.015a	13.78a	0.639a
0.001a	1.292a	0.006077a	131.98a	11.70a	0.635a
0.001a	0.771a	0.007495a	92.24b	8.30b	0.630a

Values followed by the same letter in the column do not differ (Tukey, P < 0,05).

The sediment concentration exhibited an exponential increase in yield stress (τ_y) (Figure 5), indicating an increase in sediment concentration during the transition from the solid to the liquid phases; this was attributable to yield stress. Therefore, when the cohesive particles of the saturated channel bed were detached by the yield stress, the sediment concentration increased. This finding is in accordance with Yang et al. (2014), who stated that the sediment concentration is affected by the rheological properties of the cohesive sediment, such as the yield stress.

https://doi.org/10.5194/hess-2022-275
Preprint. Discussion started: 10 August 2022

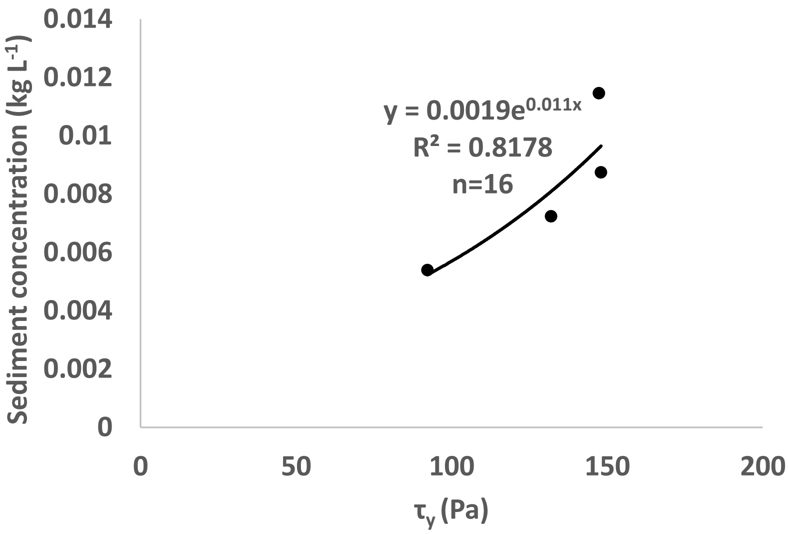

Figure 5. The exponential relationship between yield stress (τ_y) and sediment concentration (C_s) from cohesive channels under different flows was applied. Average values considering four repetitions and n (runs number) = 16.

Similarly, Figure 6 shows a sediment concentration that increases exponentially with respect to the dimensionless yield stress parameter (τ_r) for a determination coefficient (R^2) of 0.9537; this further demonstrates that the sediment concentration was affected by the yield stress. Figures 5 and 6 show that the cohesive sediment reacted similarly to the shear stresses generated by flow in the channels and by direct shear testing in the laboratory, respectively.

A strong exponential relationship ($R^2 = 0.9791$) between the Shields critical parameter (θ_{crc}) and the dimensionless particle diameter (D*) was obtained using the methodology proposed by Zhang and Yu (2017) (Figure 7). In the studies by Van Rijn (1984) and Yu and Lim (2003), θ_{crc} was negatively correlated with the dimensionless particle diameter of the alluvial channels. However, the Shields critical parameter (θ_{crc}) is a positive exponential function of the dimensionless particle diameter of the clay sediment D*, as verified by Zhang and Yu (2017).

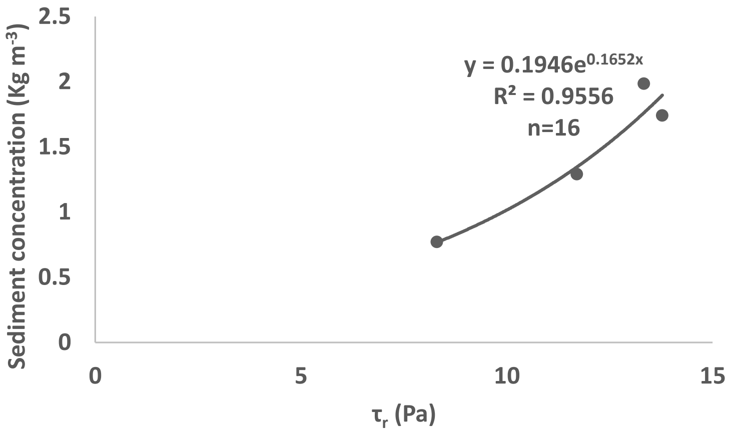

Figure 6. The exponential relationship was applied between dimensionless yield stress parameter (τr) and sediment concentration (Cs) from cohesive channels under different flows. Average values considering four repetitions and n (runs number) = 16.

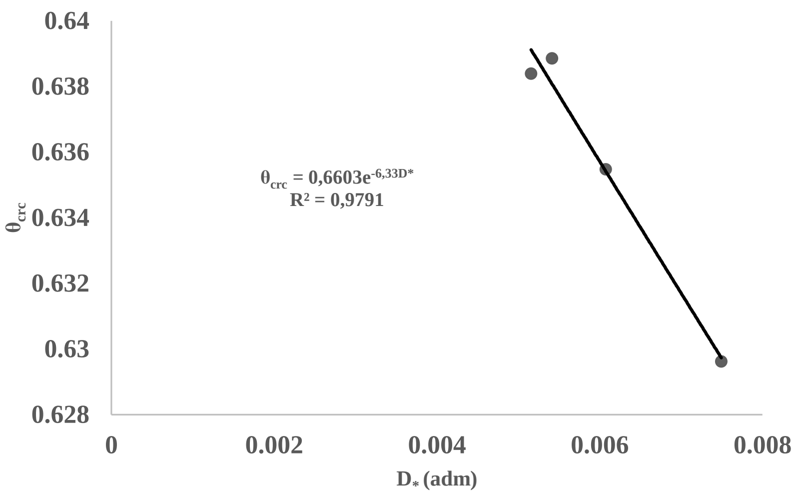

Figure 7. Cohesive Shields parameter behavior, according to the equation proposed by Zhang and Yu (2017), about the dimensionless cohesive sediment diameter.

The observed critical shear stress (τ_c) and bed erodibility (K) were obtained via a linear regression between the detachment rates and applied shear stresses, as shown in Figure 8. The bed resistance parameters, expressed by the obtained critical shear stress

https://doi.org/10.5194/hess-2022-275
Preprint. Discussion started: 10 August 2022

(τ_c) and erodibility, were inversely proportional to the shear stress tension. The critical shear stress and cohesive bed erodibility were 120 Pa and 0.00003 kg N^{-1} s^{-1}, respectively, when the critical shear stress exceeded the applied shear stress. This suggests that the shear stresses could have been higher; consequently, the straight line in Figure 8 could have been steeper.

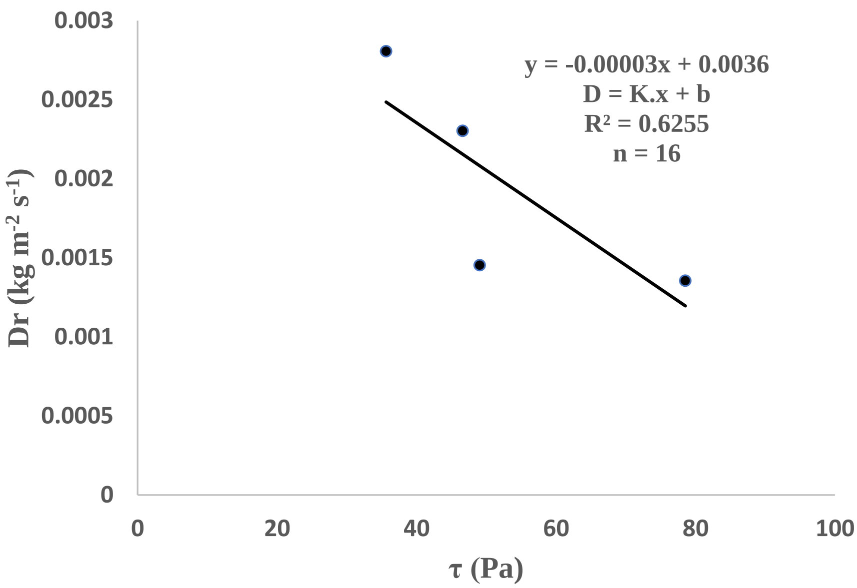

Figure 8. Relationship between soil detachment rates (D) and shear stress (τ) obtained on cohesive channels under different flows applied. Average values considering four repetitions and n (runs number) = 16.

Hanson and Simon (2001) obtained critical shear stress values ranging from 1.31 to 256 Pa for a cohesive streambed; these values are similar to the critical shear stress values obtained in this study. Simon and Thomas (2002) found similar results in the Yalobusha River Basin in Mississippi, with jet testing results indicating a range of critical shear stress values (τc) from 0 to 400 Pa and a mean value of 105 Pa. These values are close to the value of 110.8 Pa obtained in the current study. Additionally, Thoman and Niezgoda (2008), when studying the stability of cohesive channels, obtained high τ_c values between 0.11 to 15.35 Pa, and erodibility values between 0.27 to 2.38 cm^3 $N^{-1}\cdot s^{-1}$.

https://doi.org/10.5194/hess-2022-275
Preprint. Discussion started: 10 August 2022

These findings are similar to those of Geng et al. (2017), who studied the spatial variations in soil resistance (K and τ_c) under concentrated flows in 36 different soils, and who obtained K values of 0.000456–0.826 kg N^{-1} s^{-1}. These authors suggested that clay exhibited the highest resistance during wetting, owing to the greater cohesion produced by its number of bonds between clay particles, which decreases its erodibility. Garde and Raju (2000) showed that for a flat limestone material (10–20 mm thick and 40–60 mm long), the critical tractive stress is ~56 N.m^2. This suggests that in the present study (in which the predominant particles were clay, with a clay content of 60%), the critical shear stresses may take high values.

Grabowski et al. (2010) and Grabowski et al. (2011) reported that the hydrodynamic aspects of erosion and sediment transport are thoroughly understood. However, cohesive sediment erodibility has proven to be more challenging to address and predict, because interparticle attraction is influenced by many sediment properties that interact in complex ways. Wuddivira et al. (2013) reported that the detachment forces acting upon strength and erodibility under tropical conditions arise frequently in cohesive soils, and that soil erodibility is determined by the complex interactions between the clay and organic matter involved in the shear strength and erodibility, rather than by a single factor.

The applied shear stresses (τ) followed the increases in the applied flow level, reaching values between 35 and 73 Pa (Table 4). Statistical analysis indicates a statistically significant difference at the highest applied flow (Q_4 = 545 L min^{-1}). This result indicates that for cohesive channels under a cohesive Ultisol, higher flow rates are required to increase the soil detachment.

Soil cohesion is a crucial parameter for understanding the resistance behavior of cohesive channels. Thus, the shear stress and soil fatigue strength needed to produce cohesion failure (C_f), according to Mirtskhoulava (1966a), were 56135 Pa and 1964.72 Pa, respectively. The cohesion value was high, and the soil fatigue strength to rupture value reflected the high clay content (617.60 g.Kg^{-1}) of the cohesive channels at a depth of 40 cm. This high cohesion value is related to the applied shear stress; therefore, in this study, higher detachment rate values were not achieved. These results agree with those of Kothyari and Jain (2008), who observed that the threshold condition can vary with respect to the clay content, shear stress, and soil moisture.

https://doi.org/10.5194/hess-2022-275
Preprint. Discussion started: 10 August 2022

3.4 Mean velocity obtained and permissible velocity estimated by Mirtskhoulava's equation for the cohesive channels

Table 6 summarizes the observed mean velocities obtained under the applied flows, as well as the permissible velocities estimated by Mirtskhoulava's equation for cohesive channels. To estimate the permissible velocities, we used the following parameters: D_{50} = 0.959 mm, g = 9.81 m s^{-2}, m = 0.8 (considering the recently revolved channel surface), γ_w = 9771 t m^{-3}, n' = 3.84003, γ_s = 26241.8 t m^{-3}, cohesion = 56135 Pa, failure cohesion = 1964.72 Pa, σ = 17.41, and K = 0.9991; the hydraulic radius (R_h) was as stated in Table 3.

Table 6. Observed mean velocities generated by applied flows and permissible velocities estimated by Mirtskhoulava's equation on cohesive channels. Average values considering four repetitions.

Applied flows	V_m	$V_{Mirtskhoulava}$
	------------	m s^{-1} ------------
Q_1	0.789 ab	1.494 c
Q_2	0.970 a	1.523 b
Q_3	1.062 a	1.557 ab
Q_4	0.488 b	1.719 a

The observed mean velocity values only differed at higher applied flows, owing to the large, pre-formed, wetted perimeter and hydraulic radius. Thus, under increased applied flow, the shear stresses did not generate sufficient detachment to cause significant erosion.

The permissible velocities estimated by Mirtskhoulava's equation exhibited values that followed the increases in applied flow. Graf (1996) observed water flow velocities for clay materials, ranging from 1.3 m s^{-1} in clay aggregates to 2.87 m s^{-1} in dispersed clay materials. However, according to Mirtskhoulava (1991) and Wuddivira et al. (2013), clay soils with high cohesion values can support velocities ranging from 1.56 to 2.76 m s^{-1}.

The shear stresses (τ) obtained from the cohesive channels were not high enough to produce sufficient detachment, and all observed velocity values measured via the

https://doi.org/10.5194/hess-2022-275
Preprint. Discussion started: 10 August 2022

electromagnetic current meter were lower than the permissible velocities estimated by Mirtskhoulava's equation. These experimental field results indicate that Mirstkulava's equation adequately estimates the permissible velocities in cohesive channels.

3.5 Dimensional analysis and permissible velocities in cohesive channels

Dimensional analysis was performed by considering the experimental parameters involved in measuring the flow velocity in cohesive channels; these constituted the hydraulic and geometric characteristics of the cohesive channel under a concentrated flow. Twelve parameters were arranged empirically using the following mathematical relationship:

$$V_m = f\left(Q, R_h, C_s, D_r, \rho, S, f, C, C_f, \tau_f, \tau_{cr}\right). \quad (21)$$

Here, V_m = mean flow velocity (m s^{-1}), Q = liquid discharge (m^3 s^{-1}), R_h = hydraulic radius (m), C_s = sediment concentration (kg L^{-1}), D = detachment rate from the concentrated flow (kg m^{-2} s^{-1}), ρ = water density (kg m^{-3}), S = channel slope (m m^{-1}), f = the Darcy–Weisbach hydraulic resistance coefficient (dimensionless), C = cohesion coefficient (Pa), C_f = failure cohesion (Pa), τ = flow shear stress (Pa), and τ_{cr} = critical shear stress (Pa).

According to Fox et al. (2014), when applying the π value or Buckingham theorem for dimensional analysis, the dimensions L, M, and T are considered fundamental for specifying the dimensions of each of the parameters involved, as follows: $[V_m] = L\ T^{-1}$, $[Q] = L^3\ T^{-1}$, $[R_h] = L$, $[C_s] = M\ L^{-3}$, $[D] = M\ L^{-2}\ T^{-1}$, $[\rho] = M\ L^{-3}$, $[C] = M\ L^{-1}\ T^{-2}$, $[C_f] = M\ L^{-1}\ T^{-2}$, $[\tau_f] = M\ L^{-1}\ T^{-2}$, $[\tau_{cr}] = M\ L^{-1}\ T^{-2}$; the remaining S and f are dimensionless.

By analyzing the chosen parameters and π properties, we observed that the channel slope (S) and Darcy–Weisbach hydraulic resistance coefficient (f) are already π terms, because they are dimensionless and correspond to π_4 and π_5, respectively. Because the variables had the same reference dimensions, other π terms were observed, such as the water density (ρ), sediment concentration (C_s), cohesion coefficient (C), failure cohesion (C_f), shear stress of the flow (τ), and critical shear stress (τ_c). Accordingly, to determine the remaining two groups, the parameters V_m, R_h, and C_s were considered repetitive, and π_1 and π_2 were thus determined.

https://doi.org/10.5194/hess-2022-275
Preprint. Discussion started: 10 August 2022

Hydrology and Earth System Sciences
Open Access
EGU
Discussions

Because we utilized 10 dimensional variables (k = 10) and three dimensions (M, L, and T) to describe the physical process, the difference between the number of dimensional variables (k) describing a process and the number of reference dimensions (r) resulted in seven dimensionless groups, as follows:

$$\pi_1 = \frac{Q}{VR_h^2}, \quad (22)$$

$$\pi_2 = \frac{D_r}{VC_s}, \quad (23)$$

$$\pi_3 = \frac{\rho}{C_s}, \quad (24)$$

$$\pi_4 = S, \quad (25)$$

$$\pi_5 = f, \quad (26)$$

$$\pi_6 = \frac{C}{C_f}, \quad (27)$$

$$\pi_7 = \frac{\tau_f}{\tau_c}. \quad (28)$$

Thus, the results were arranged into π groups as

$$\pi_1 = f(\pi_2, \pi_3, \pi_4, \pi_5, \pi_6, \pi_7), \quad (29)$$

and in a dimensionless group arrangement, as

$$\frac{Q}{VR_h^2} = f\left(\frac{D_r}{VC_s}, \frac{\rho}{C_s}, S, f, \frac{C}{C_f}, \frac{\tau_f}{\tau_c}\right). \quad (30)$$

Finally, the dimensionless terms made it possible to calculate the π numerical values, as summarizes in Table 7, as well as to proceed with regression analyses and obtain a new model. All terms obtained (except π_6) varied, which corresponded to the relationship between two constant parameters throughout the experiment. Considering all this information, several relationships pertaining between the dimensionless parameters were tested, as shown in Figure 9.

Figure 9 shows the linearity of the relationships between π_1 and π_2 and π_1 and π_5 ($R^2 = 0.9978$ and $R^2 = 0.9221$, respectively) and the exponential relationship between π_1 and π_3 and π_1 and π_7. There was no correlation between π_1 and π_6; consequently, π_6 was not considered in the model development; however, we included 16 runs for each variable.

https://doi.org/10.5194/hess-2022-275
Preprint. Discussion started: 10 August 2022

Hydrology and Earth System Sciences Discussions
Open Access
EGU

Table 7. Numerical values corresponding to the π terms obtained from cohesive channels represent the flow velocities.

Runs	π_1	π_2	π_3	π_4	π_5	π_6	π_7
1	6.75E-07	0.020	325.65	0.161	0.800	33.192	3.006
2	1.16E-06	0.006	505.63	0.141	0.400	33.192	2.906
3	4.76E-07	0.002	748.40	0.128	0.370	33.192	3.811
4	5.40E-07	0.005	640.98	0.128	0.355	33.192	4.019
5	8.72E-07	0.012	317.29	0.188	0.405	33.192	2.206
6	9.96E-07	0.002	762.90	0.161	0.394	33.192	2.537
7	1.05E-06	0.005	534.25	0.141	0.356	33.192	2.950
8	7.64E-07	0.001	1588.59	0.168	0.398	33.192	2.720
9	1.08E-06	0.002	689.24	0.154	0.217	33.192	2.302
10	1.43E-06	0.002	710.18	0.179	0.472	33.192	2.060
11	1.42E-06	0.002	774.47	0.121	0.335	33.192	3.029
12	8.70E-07	0.001	983.16	0.158	0.429	33.192	2.592
13	6.14E-05	0.001	1889.61	0.161	2.970	33.192	1.278
14	4.27E-05	0.002	1476.99	0.161	2.732	33.192	1.358
15	7.26E-05	0.004	1088.94	0.128	4.900	33.192	1.575
16	3.50E-05	0.002	1041.49	0.094	1.223	33.192	2.153

https://doi.org/10.5194/hess-2022-275
Preprint. Discussion started: 10 August 2022

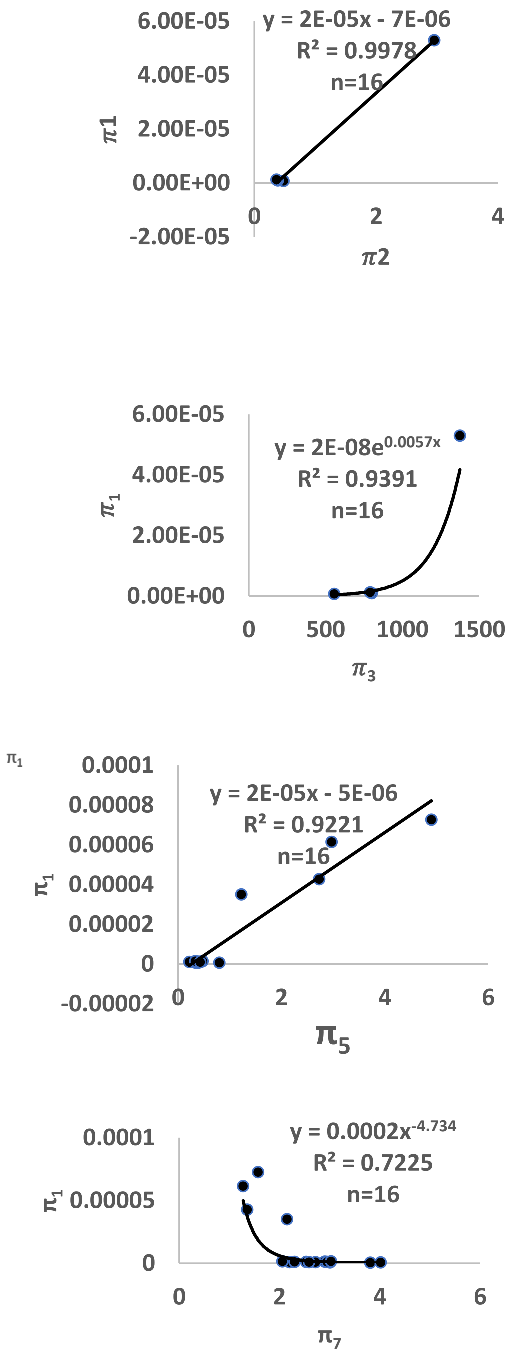

Figure 9. Relationships between the terms π dimensionless, dependent, and independents represent the mean velocities obtained from cohesive channels in 16 runs.

https://doi.org/10.5194/hess-2022-275
Preprint. Discussion started: 10 August 2022

Hydrology and Earth System Sciences
Discussions
Open Access

Table 8 summarizes the permissible velocity values obtained via the dimensional analyses that yielded the π_1 term and the permissible velocity values calculated using the equation proposed by Mirtskhoulava (1991) [Eq. (7)]. The average difference between the permissible velocities calculated from the Mirtshloulava equation and π_1 term equation was only 17.24% of the 16 cohesive channels under increasing applied flows. These obtained velocity values are in accordance with Mirtskhoulava (1991); however, the clay soils with cohesion values varying between 5×10^4 Pa had assumed permissible velocities of 1.56–2.72 m s^{-1} in the channels exhibiting cohesion values of 5.6×10^4 Pa.

Table 8. Permissible velocities (m s^{-1}) were calculated according to Mirtskhoulava (1966b), and the π_1 term was produced from hydraulic variables obtained on cohesive channels with 60% clay content.

Permissible velocity Mirtskhoulava (1966b)	Permissible velocity $\pi 1\left(\frac{Q}{VR_h^2}\right)$	Difference (%)
1.38	1.11	19.57
1.42	1.41	0.70
1.38	1.04	24.64
1.37	1.45	5.84
1.42	1.26	11.27
1.42	1.29	9.15
1.42	1.42	0
1.39	1.48	6.47
1.46	1.14	21.92
1.45	1.23	15.17
1.45	1.17	19.31
1.42	1.07	24.65
1.60	2.63	64.38
1.58	2.36	49.37
1.60	1.97	23.13
1.60	1.68	1.88

Permissible velocity equations, such as the Mirtshloulava equation [Eq. (7)] and the π_1 equation [Eq. (20)], were developed to predict the highest velocity that a flow can reach without detaching the cohesive surface channel; however, the permissible velocity values obtained (Table 8), based on the shear stress values (Tables 3 and 4) applied in this study, were not sufficient to increase the detachment rate values.

3.6 Multiple regression

A multiple regression of the π terms was obtained without π_6, which was constant. Thus, the dependent variable Y corresponded to X1, X2, X3, X4, and X6. Table 9 summarizes the correlation matrix for π terms.

https://doi.org/10.5194/hess-2022-275
Preprint. Discussion started: 10 August 2022

Table 9. Correlation coefficient matrix for π terms in dimensionless terms.

Variables	$\pi 2$ $(\frac{D_r}{VC_S})$	$\pi 3$ $(\frac{\rho}{C_S})$	$\pi 4$ (S)	$\pi 5$ (f)	$\pi 7$ $(\frac{\tau_f}{\tau_c})$	$\pi 1$ $(\frac{Q}{VR_h^2})$
$\pi 2$ $(\frac{D_r}{VC_S})$	**1**	-0.614	0.217	-0.114	0.221	-0.225
$\pi 3$ $(\frac{\rho}{C_S})$	-0.614	**1**	0.006	0.549	-0.556	0.647
$\pi 4$ (S)	0.217	0.006	**1**	-0.132	-0.304	-0.224
$\pi 5$ (f)	-0.114	0.549	-0.132	**1**	-0.680	0.960
$\pi 7$ $(\frac{\tau_f}{\tau_c})$	0.221	-0.556	-0.304	-0.680	**1**	-0.727
$\pi 1$ $(\frac{Q}{VR_h^2})$	-0.225	0.647	-0.224	0.960	-0.727	**1**

Significance level: p < 0,05.

In the regression method, a high coefficient determination was obtained, suggesting a 98% dependent variable variability, which was explained using the five independent variables, as shown below:

$$\pi_1 = (4.75)10^{-5} + (3.71\pi_2)10^{-4} + (1.02\pi_3)10^{-5} - (2.40\pi_4)10^{-4} + (1.20\pi_5)10^{-5} - (9.73\pi_7)10^{-6} \,. \quad (31)$$

Substituting the π terms via the variables applied in the dimensional analyses produced

$$\frac{Q}{VR_h^2} = (4.75)10^{-5} + \left(3.71\frac{D_r}{VC_s}\right)10^{-4} + \left(1.02\frac{\rho}{C_s}\right)10^{-5} - (2.4\,\mathrm{S})10^{-4} + (1.20\,f)10^{-5} - \left(9.73\frac{\tau_f}{\tau_c}\right)10^{-6}, \quad (32)$$

which predicts the permissible velocity in cohesive channels.

The regression model performed well under field conditions in the cohesive channels for the applied flows and observed hydraulic variables; however, the latter variables should be tested under higher-level flows.

4. Conclusions

Based on the flows applied to cohesive channels in the field experiment, the following conclusions can be drawn:

The soil resistance expressed by the critical shear stress (τ_c) and erodibility was inversely proportional to the applied shear stress tension. In addition, a critical shear stress

https://doi.org/10.5194/hess-2022-275
Preprint. Discussion started: 10 August 2022

and channel erodibility of 120 Pa and 0.00003 kg N^{-1} s^{-1}, respectively, were observed for the cohesive channel under the B-horizon of Ultisol, higher than the shear stress generated by the applied flows. This suggests that the applied shear stress flows could have been higher, and that higher soil detachment rates could have been realized.

The high cohesion value obtained and the soil fatigue strength to rupture value reflected the high clay content (617.60 g/Kg) of the cohesive channels. These cohesion values were related to the applied shear stress.

The yield stress was significant for the geometric alteration, flow velocity, and sediment concentration of the cohesive channels under the highest applied flow.

These results indicate that Mirstkulava's equation performed adequately in this field experiment when estimating the permissible velocities on cohesive channels.

The dimensional analysis applied to the obtained hydraulics variables produced the following equation, which predicts the permissible velocity in cohesive channels:

$$\frac{Q}{VR_h^2} = (4.75)10^{-5} + \left(3.71\frac{D_r}{VC_s}\right)10^{-4} + \left(1.02\frac{\rho}{C_s}\right)10^{-5} - (2.4\ \mathrm{S})10^{-4} + (1.20\ f)10^{-5} - \left(9.73\frac{\tau_f}{\tau_c}\right)10^{-6}. \quad (32)$$

This regression model performed well under field conditions in the cohesive channels for level-applied flows and observed hydraulic variables; however, the latter variables need to be tested under higher-level flows. We hope that this study will serve as a technical reference for engineers seeking to build effective, appropriate river structures in cohesive channels.

Statements and Declarations

There is no interest conflict and no disclosed or non-financial interests related to submitting this manuscript and future publication between the authors.

This work was supported by **CAPES**, Brazil (Coordenação de Aperfeiçoamento de Pessoal de Nível superior), and **FACEPE** (Fundação de Amparo à Ciência e Tecnologia do Estado de Pernambuco).

References

Aliev, T.A. Canals in cohesive soils. Hydrotechnical Construction, 19, 301–307, https://doi-org.nottingham.idm.oclc.org/10.1007/BF02028562, 1985.

https://doi.org/10.5194/hess-2022-275
Preprint. Discussion started: 10 August 2022

Al-Hamdan, O.Z., Pierson, F.B., Nearing, M.A., Williams, C.J., Stone, J.J., Kormos, P.R., Boll, J., & Weltz, M.A. Risk Assessment of Erosion from Concentrated Flow on Rangelands Using Overland Flow Distribution and Shear Stress Partitioning. Transactions of the ASABE, 56, 539–548, https://doi.org/10.13031/2013.42684, 2013.

Ansari, S.A., Kothyari, U.C., & Raju, K.G.R. Influence of Cohesion on Scour under Submerged Circular Vertical Jets. Journal of Hydraulic Engineering, 129,12, 1014–1019, https://doiorg.nottingham.idm.oclc.org/10.1061/(ASCE)07339429(2003)129:12(1014), 2003.

ASTM D 3080-98. Standard test method for direct shear test of soils under consolidated drained conditions. Annual Book of ASTM Standards, 04.08. https://doi.org/10.1520/D3080-04, 2003.

Bezerra, S. A., Cantalice, J. R. B., Filho, M. C., Souza, & W. L. da S. Características hidráulicas da erosão em sulcos em um Cambissolo do semiárido do Brasil. Revista Brasileira de Ciência do Solo, 34, 1325–1332. https://doi.org/10.1590/S0100-06832010000400029, 2010.

Blake, G.R., & Hartge, K.H. Particle density, in: A. Klute, (Ed.): Methods of Soil Analysis: Part 1—Physical and Mineralogical Methods. Second ed., 377–382, American Society of Agronomy, 1986.

Cantalice, J.R. B., Silveira, F. P. M., Singh, V. P., Silva, Y. J. A. B., Cavalcante, D. M., & Gomes, C. Interrill erosion and roughness parameters of vegetation in rangelands. Catena, 148,2, 111–116. https://doiorg.nottingham.idm.oclc.org/10.1016/j.catena.2016.04.024, 2017.

Cassol, E.A., Cantalice, J.R.B., Reichert, J.M., & Mondardo, A. Escoamento superficial e desagregação do solo em entressulcos em solo franco-argilo-arenoso com resíduos vegetais. Pesquisa Agropecuária Brasileira, 39, 685–690. https://doi.org/10.1590/S0100-204X2004000700010, 2004.

De Baets, S., Poesen, J., Gyssels, G., & Knapen, A. Effects of grass roots on the erodibility of topsoils during concentrated flow. Geomorphology, 76,1–2, 54–67. https://doi-org.nottingham.idm.oclc.org/10.1016/j.geomorph.2005.10.002, 2006.

https://doi.org/10.5194/hess-2022-275
Preprint. Discussion started: 10 August 2022

Hydrology and Earth System Sciences
Open Access
Discussions

Díaz, Rafael P. Sacsa. Análise Dimensional e Simulação da Transferência de Calor e Massa em Reservatórios de Gás Natural Adsorvido. Tese (Doutorado em Engenharia Mecânica). Universidade Federal Fluminense, Niterói, Brasil, 2012.

Dym, C. L., Little, P., Orwin, E. J., & Spjut, R. E. Introdução à Engenharia: Uma Abordagem Baseada em Projeto. Bookman, 2010.

Elliot, W.J., Liebenow, A.M., Laflen, J.M., & Kohl, K.D. A compendium of soil erodibility data from WEPP cropland soil field erodibility experiments 1987 & 88. National Soil Erosion Research Laboratory, 1989.

Farenhorst, A., Bryan, R.B. Particle size distribution of sediment transported by shallow flow. Catena, 25(1–4), 47–62. https://doi.org/10.1016/0341-8162(94)00041-C, 1995.

Flanagan, D.C. & Nearing, M.A. Erosion Prediction Project, Hillslope Profile and Watershed Model Documentation. United States Department of Agriculture, 1995.

Flint, L.E. & Flint, A.L. Porosity. In: J.H. Dane & C.G. Topp, (Eds.): Methods of Soil Analysis: Part 4. Physical Methods,Second ed., pp. 241–253, Soil Science Society of America, 2002.

Fox, R. W., Mcdonald, A. T., Pritchard, P. J. & Leylegian, J. C. Introduction to fluid mechanics. John Wiley & Sons, 2014.

Garde, R.J. & Raju., K.R. Mechanics of sediment transportation and alluvial stream problems. Taylor & Francis, 20000.

Geng, R., Zhang, G., Ma, Q., & Wang, L. Soil resistance to runoff on steep croplands in Eastern China. Catena, 152, 18–28. https://doi.org/10.1016/j.catena.2017.01.002, 2017.

Grabowski, R. C., Droppo, I.G., & Wharton, G. Estimation of critical shear stress from cohesive strength meter-derived erosion thresholds. Limnology and Oceanography: Methods, 8,12, 678–685. https://doi.org/10.4319/lom.2010.8.678, 2010.

Grabowski, R.C., Droppo, I.G., & Wharton, G. (2011). Erodibility of cohesive sediment: The importance of sediment properties. Earth-Science Reviews, 105,3–4, 101–120. https://doi.org/10.1016/j.earscirev.2011.01.008, 2011.

Graf, W.H. Hydraulics of Sediment Transport. Water Resources Publications, 1984.

Grossman, R.B. & Reinsch, T.G. Bulk Density and Linear Extensibility. In J.H. Dane & C.G. Topp (Eds.): Methods of Soil Analysis: Part 4. Physical Methods. pp. 201-214, Soil Science Society of America, 2002.

https://doi.org/10.5194/hess-2022-275
Preprint. Discussion started: 10 August 2022

Hanson, G. J. & Simon, A. Erodibility of cohesive streambeds in the loess area of the midwestern USA. Hydrological Processes, 15,1, 23–38. https://doi-org.nottingham.idm.oclc.org/10.1016/j.earscirev.2011.01.008, 2001.

Jain, R.K. & Kothyari, U.C. Cohesion influences on erosion and bed load transport. Water Resources Research, 45,6,1–17. https://doiorg.nottingham.idm.oclc.org/10.1029/2008WR007044, 2009.

Julien, P.Y. Erosion and Sedimentation. Cambridge University Press, 1995.

Khanal, A., Klavon, K.R., Fox, G.A., & Daly, E.R. Comparison of Linear and Nonlinear Models for Cohesive Sediment Detachment: Rill Erosion, Hole Erosion Test and Streambank Erosion Studies. Journal of Hydraulic Engineering, 142,9, 1–12. https://doi-org.nottingham.idm.oclc.org/10.1061/(ASCE)HY.1943-7900.0001147, 2016.

Kothyari, U. C. & Jain, R. K. Influence of cohesion on the incipient motion condition of sediment mixtures. Water Resources Research, 44, https://doi-org.nottingham.idm.oclc.org/10.1029/2007WR006326, 2008.

Mahalder, B., Schwartz, J. S., Palomino, A. N., Zirkle, J. Estimating Erodibility Parameters for Streambanks with Cohesive Soils Using the Mini Jet Test Device: A Comparison of Field and Computational Methods. Water, 10, 304. https://doi.org/10.3390/w10030304, 2018.

Mirtskhoulava, T.E. Studies on permissible velocities for soil and facings. Modern trends in Hydraulic Engineering Research, Central Water and Power Research Station, Poona. vol. 1, 1996.

Mirtskhoulava, T.E. (1991). Scouring by flowing water of cohesive and noncohesive beds. Journal of Hydraulic Research, 29, 341–354. https://doiorg.nottingham.idm.oclc.org/10.1080/00221689109498438, 1991.

Munson. B. R., Young. D. F., Okiishi. T. H. Análise dimensional e modelos. Fundamentos da mecânica dos fluidos, 4th ed., 344–397. Edgard Blücher, 2004.

Thoman, R. W. & Niezgoda, S. L. Determining Erodibility, Critical Shear Stress, and Allowable Discharge Estimates for Cohesive Channels: Case Study in the Powder River Basin of Wyoming. Journal of Hydraulic Engineering, 134,12. https://doiorg.nottingham.idm.oclc.org/10.1061/(ASCE)0733-9429(2008)134:12(1677), 2008.

https://doi.org/10.5194/hess-2022-275
Preprint. Discussion started: 10 August 2022

Partheniades, E. Erosion and deposition of cohesive soils. Journal of Hydraulic Division, 91, 105–138. https://doiorg.nottingham.idm.oclc.org/10.1061/JYCEAJ.0001165, 1965.

Qasem, S. N., Ebtehaj, I., & Madavar, H. R. Optimizing ANFIS for sediment transport in open channels using different evolutionary algorithms. Journal of Applied Research in Water and Wastewater, 4, 290–298. https://dx.doi.org/10.22126/arww.2017.773, 2017.

Sekine, M., Nishimori, K., Masato, S., & Ken-ichiro, N. Erosion rate of cohesive sediment by running water. Fourth International Conference on Scour and Erosion, 424–429, 2008.

Simons, D.B. & Senturk, F. Sediment transport technology: water and sediment dynamics. Water Resources Publication, USA, 1992.

Simon, A., & Thomas, R. E. Processes and forms of an unstable system with resistant, cohesive streambeds. Earth Surface Processes and Landforms, 27, 699–718. https://doiorg.nottingham.idm.oclc.org/10.1002/esp.347, 2002.

Slattery, M.C. & Bryan, R.B. Hydraulic conditions for rill incision under simulated rainfall: A laboratory experiment. *Earth Surface Processes and Landforms*, 17, 127–146. https://doi-org.nottingham.idm.oclc.org/10.1002/esp.3290170203, 1992.

USDA, Soil Survey Staff. Keys to Soil Taxonomy, 8th edition, USDA-NRCS, USA, 1998.

Yang, W., Yu, G., Tan, S. K., & Wang, H. Rheological properties of dense natural cohesive sediments subject to shear loadings. International Journal of Sediment Research, 29, 454–470. http://dx.doi.org/10.1016/S1001-6279(14)60059-7, 2014.

Yu, G. & Lim., S. Modified manning formula for flow in alluvial channels with sand-beds. Journal of Hydraulic Research, 41, 597–608. http://dx.doi.org/10.1080/00221680309506892, 2003.

Thoman, R. W. & Niezgoda, S. L. Determining Erodibility, Critical Shear Stress, and Allowable Discharge Estimates for Cohesive Channels: Case Study in the Powder River Basin of Wyoming. *Journal of Hydraulic Engineering*, 134(12), 1677-1687. https://doi-org.nottingham.idm.oclc.org/10.1061/(ASCE)07339429(2008)134:12(1677), 2008.

Utley, B.C. & Wynn, T.M. Cohesive Soil Erosion: Theory and Practice. World Environmental and Water Resources Congress, https://doi-org.nottingham.idm.oclc.org/10.1061/40976(316)289, 2008.

https://doi.org/10.5194/hess-2022-275
Preprint. Discussion started: 10 August 2022

Van Rijn, L. C. Sediment transport, part I: Bed load transport. Journal of Hydraulic Engineering, 110, 1431–1456. https://doiorg.nottingham.idm.oclc.org/10.1061/(ASCE)0733-9429(1984)110:10(1431), 1984.

Wuddivira, M.N., Stone, R.J., & Ekwue, E.I. Influence of cohesive and disruptive forces on strength and erodibility of tropical soils. Soil Tillage Research, 133, 40–48. https://doi-org.nottingham.idm.oclc.org/10.1016/j.still.2013.05.012, 2013.

Zhang, M. & Yu, G. (2017). Critical conditions of incipient motion of cohesive sediments. Water Resources Research, 53, 7798–7815. https://doi-org.nottingham.idm.oclc.org/10.1002/2017WR021066, 2017.

Zhang, M., Yu, G., Rovery, A. L., & Ranzi, R. Erodibility of fluidized cohesive sediments in unidirectional open flow. Ocean Engineering, 130, 523–530. http://dx.doi.org/10.1016%2Fj.oceaneng.2016.12.021, 2017.